# Widespread Mitochondrial DNA Methylation Drift Contributes to Postoperative Delirium in Young and Old Mice

**Yue Liu**
Nanjing University Medical School Affiliated Nanjing Drum Tower Hospital
**Shuai Yang**
Nanjing University Medical School Affiliated Nanjing Drum Tower Hospital
**Wei Zhang**
Nanjing University Medical School Affiliated Nanjing Drum Tower Hospital
**Yan Yang**
Nanjing University Medical School Affiliated Nanjing Drum Tower Hospital
**Ming Jiang**
Nanjing University Medical School Affiliated Nanjing Drum Tower Hospital
**Zhengliang Ma** ( mazhengliang1964@163.com )
Department of Anesthesiology, Affiliated Drum Tower Hospital of Medical School of Nanjing University, 321 Zhongshan Road, Nanjing 210008, Jiangsu province, China https://orcid.org/0000-0002-1000-4123
**Xiaoping Gu**
Nanjing University Medical School Affiliated Nanjing Drum Tower Hospital

**Research**

**Keywords:** mitochondrial DNA methylation, postoperative delirium, aging, prefrontal cortex, hippocampus

**Posted Date:** October 2nd, 2020

**DOI:** https://doi.org/10.21203/rs.3.rs-84137/v1

# Abstract

**Background:** Mitochondrial dysfunction is linked to the etiopathogenesis of postoperative delirium (POD), which severely affects the prognosis of elderly patients undergoing surgery. The methylation of mitochondrial DNA (mtDNA), a new and incompletely described phenomenon that regulates the structure and function of mitochondria, is associated with aging. However, the relationship between mtDNA methylation and POD has not been established.

**Methods:** 5-methylcytosine (5-mC) at 5 CpG sites of the displacement loop (D-loop) and at 60 CpG sites of coding gene loci in the mitochondrial genome after surgery of the hippocampus, prefrontal cortex, amygdala, and anterior cingulate cortex in 6- and 18-month-old mice were detected using bisulfite pyrosequencing. Mitochondrial structure, mitochondrial gene expression and mtDNA copy number were also examined using Electron microscopy and real time PCR to find the association with mtDNA methylation

**Results:** The mtDNA methylation drift manifested as a decrease in the methylation levels at the D-loop and an increase or decrease in the methylation levels at several coding gene loci, ultimately resulting in reduced mtDNA copy numbers, altered mitochondrial gene expression, and damaged mitochondrial structures in the hippocampus and prefrontal cortex after surgery. The activation of Silent information regulator-1 (SIRT1) ameliorated anesthesia- and surgery-induced mitochondrial dysfunction and delirium-like behaviors by regulating mtDNA methyltransferase-mediated mtDNA methylation.

**Conclusions:** These data support the existence of epigenetic mtDNA regulation in POD; however, further studies are required to explore the specific mechanisms.


# Introduction

Postoperative delirium (POD) is a common postoperative complication manifesting as acute and fluctuating disturbances in cognition, consciousness, and attention, mainly occurring in hours to days after surgery [1]. Age is an important risk factor and predictor for the development of POD [2]. The incidences of POD in elderly patients after major abdominal surgery and cardiac surgery are approximately 50% and 51% respectively [3, 4]. POD can cause increased short-term and long-term postoperative complications or functional impairment (such as a 10-fold increase in the risk of postoperative cognitive dysfunction), prolonged intensive care and hospital stays, and 2- to 20-fold increases in postoperative mortality [1, 5, 6]. However, the neuropathogenesis of POD is not well understood. Therefore, its clinical diagnosis mainly depends on scale assessments, such as the Confusion Assessment Method (CAM) [7], which lacks the sensitivity of laboratory examinations for early diagnosis or screening susceptible populations. Furthermore, effective prevention and targeted treatment remain largely to be determined.

Anesthesia- and surgery-induced mitochondrial dysfunction, which leads to energy deficits and oxidative stress in the cortex, plays important roles in behavioral changes in mouse models of POD [8].

Mitochondria contain their own maternally inherited DNA (mitochondrial DNA [mtDNA]), which is circular, double-stranded, and approximately 16 kb in size [9]. mtDNA encodes 13 protein components for the oxidative phosphorylation system, including seven subunits of complex I (NADH dehydrogenase subunits ND1, ND2, ND3, ND4, ND4L, ND5, and ND6), one subunit of complex III (cytochrome b), three subunits of complex Ⅳ (cytochrome oxidase: COX1, COX2, and COX3), and two subunits of complex Ⅴ (ATPase 6 and ATPase 8). mtDNA also encodes 22 transfer RNAs and two ribosomal RNAs (rRNAs) for translation of polypeptides in the mitochondria [10]. The displacement loop (D-loop), which is the only noncoding region in mtDNA, regulates mitochondrial transcription and replication [10]. Compared with nuclear DNA, mtDNA lacks protective nucleosomes, histones, and an efficient DNA repair system and is therefore more susceptible to changes in the external and internal environments. In particular mtDNA is susceptible to reactive oxygen species (ROS), which are established determinants of DNA methylation modification on cytosine residues [11, 12]. Although not completely characterized, emerging findings have indicated that 5-methylcytosine (5-mC) in mtDNA can be detected in approximately 2–18% of CpG and non-CpG sites using bisulfite conversion and pyrosequencing, and mitochondrially targeted DNA methyltransferase 1 (DNMT1) and DNMT3A are suggested to be responsible [13, 14].

Moreover, alterations in mitochondrial genome methylation are known to play important roles in mtDNA gene expression and replication, thereby directly affecting the oxidative phosphorylation system and regulating the structure and function of mitochondria [15, 16]. mtDNA methylation drift, which includes both gains and losses in methylation at various sites, is conserved across species and associated with aging, environmental exposure, and metabolic and neurodegenerative diseases, such as Alzheimer's disease, Parkinson's disease, and diabetic retinopathy [17–19]. Recent studies have suggested that blood mtDNA methylation at CpG sites could be used as an epigenetic biomarker of aging [20]. In prefrontal cortex (PFC) samples, mtDNA methylation at most elements decreases significantly with age. Thus, mtDNA copy numbers and mitochondrial gene expression increase and decrease with age, respectively [13]. However, no data have reported mitochondrial 5-mC levels in specific brain regions associated with cognition, consciousness, attention, and emotion, such as the PFC, hippocampus, amygdala, and anterior cingulate cortex (ACC), in postoperative delirium.

In this study, we explored the potential roles of mitochondrial epigenetic regulation in POD using young and old mice. Our findings provided important insights into the functional significance of mtDNA methylation modification in POD.

## Materials And Methods

# Animals

Young and old male C57BL/6N mice (6 and 18 months old, respectively) were used in this study. Six-month-old mice were provided by the Laboratory Animal Center of Nanjing Medical University and housed at the Animal Facility of Drum Tower Hospital until they reached 18 months of age. All mice were housed in a climate-controlled room (22 ± 2 °C), with a 12-h reversed light/dark cycle starting at 06:00 h. Food

and water were provided *ad libitum*. Experimental procedures were approved by the Institutional Animal Care and Use Committee of Nanjing University. All applicable institutional and/or national guidelines for the care and use of animals were followed. Every effort was made to minimize animal suffering and to use the minimum number of mice necessary for obtaining valid results.

# Anesthesia and surgery for establishing the mouse model of POD

Mice were randomly assigned to different groups. The mouse model of POD was established as previously described [8]. The anesthesia and surgery procedures were started between 6:00 and 8:00 am. Briefly, mice were anesthetized with inhalation of isoflurane (1.4% in 100% oxygen for induction and maintenance; Hengrui, Shanghai, China) in a transparent anesthetizing chamber. Ten minutes after anesthesia induction, mice were moved out of the anesthetizing chamber, and anesthesia was maintained via a nose mask. The abdominal area was shaved and sterilized with 5% povidone-iodine solution. Then, a longitudinal midline incision was made starting at the xiphoid and extending towards 0.5 cm from the proximal pubic symphysis on the skin, abdominal muscles, and peritoneum. The incision was sutured layer by layer using 5–0 nylon. The wound site was covered with compound 2.5% prilocaine and 2.5% lidocaine cream (Tongfang, Beijing, China) at the end of surgery and then every 8 h for 2 days to alleviate incisional pain. The surgery for each mouse lasted approximately 10 min. Mice were then placed back into the chamber, and isoflurane anesthesia was maintained for 2 h. Heart rate, respiratory rate, oxygen saturation, and body temperature were monitored and maintained within normal levels during the procedure (MouseOx Monitor; STARR Life Science Corp., Oakmont, PA, USA). At the same time, control mice stayed in their cages with room air for 2 h.

# Behavioral tests

Behavioral tests were performed in the following order: buried food finding test, open field test, Y maze test, and nonselective nonsustained attention test (NNAT), at 24 h before surgery and at 6, 9, and 24 h after surgery. The series of tests for each mouse lasted 20 min, and tests for all mice at each time point were finished within 50 min in order to minimize any possible influence of time factors. After each test, the apparatuses were cleaned with 75% ethanol solution. Behavioral tests and video analysis were performed by experimenters who were blinded to the study design and grouping.

# Buried food finding test

The buried food finding test was performed according to a previous method with modifications [21]. Briefly, mice were given two pieces of sweetened cereal 48 h before the test. Mice were placed in the home cage in the testing room for 1 h to acclimatize before the test on the test day. The test cage (38 × 17 × 18 cm) was prepared with clean bedding (3 cm thick) for each mouse. A piece of cereal was hidden 0.5 cm beneath the surface of the bedding in a corner of the test cage. The location was changed every time randomly. Each mouse was then placed in the opposite corner, and the time required for the mouse to find the food was measured. Latency was defined as the time from when the mouse was positioned in the test cage to when the mouse uncovered the food and initiated eating. The test was performed during

a 5-min period. If the mouse could not find the food within 5 min, the test ended, and the latency was recorded as 300 s.

# Open field test

The open field test was performed as previously described with modifications [8]. Prior to the test day, mice were allowed to acclimatize for 1 h. On the day of testing, each mouse was placed in the center of the open field chamber (40 × 40 × 40 cm) under dim light and was allowed free movement for 5 min. Parameters, including the total distance traveled (cm), time spent in the center zone of the open field (s), freezing time (s), and the time until the mouse entered the center zone at the first attempt (s), were assessed and analyzed via a video camera linked to the PanlabSMART animal tracking system software (RWD Life Science Co., Shenzhen, China). The central zone was defined as the 20 × 20 cm area located in the center of the open field.

# Y maze test

The Y maze test was performed as previously described with modifications [8]. The Y maze consisted of three arms (33 × 15 × 10 cm) made of the same black plastic positioned at equal angles. The starting arm, in which the mice started to explore, was always open. The novel arm was blocked during the first trial, but open during the second trial. The other arm was always open. The first trial was a training session the mouse was allowed to explore the starting arm and the other arm for 10 min (the novel arm was closed). After a 2-h interval, the second trial was performed; the mouse was placed back into the same start arm and allowed to explore all three arms freely for 5 min. The time spent in and the number of entries into the novel arm were recorded and analyzed via a video camera linked to the PanlabSMART animal tracking system software (RWD Life Science Co.).

# NNAT

The NNAT was performed as previously described with modifications [22]. The open field chamber (40 × 40 × 40 cm) was placed in a quiet room under dim white light. The floor was equally divided into nine squares. Four familiar objects with the same diameter (1.5 cm), color, texture, and shape were placed at the four angles of the central square. During the familiarization period prior to the test day, mice were individually introduced into the chamber containing the four familiar objects for 5 min/day on three consecutive days. On the test day, one of the familiar objects was replaced with a new object with the same size, color, and texture but a different shape. Mice were individually allowed to explore in the chamber freely for 5 min. The time spent exploring the objects was video recorded. The attentional level was the percentage of duration of exploration of the new object in comparison with the total time spent exploring all four objects.

All data for the behavior tests were presented as percentages compared with baseline for the same group. Z score was calculated using the following formula, as previously described [23]:

$$Z\ score = (\Delta X\ [treatment] - mean\ \Delta X\ [control]) / SD\ \Delta X\ (control)$$

where ΔX (treatment) and ΔX (control) were the change scores at different time points after treatment or control procedure minus the scores at the baseline, respectively. The composite Z score for each mouse was calculated as the sum of the seven Z scores (latency to eat food, time spent in the center, freezing time, latency to the center, entries in the novel arm, duration in the novel arm, and attention level), normalized to the SD for that sum in the control group. Some Z scores (time spent in the center, freezing time, entries in the novel arm, duration in the novel arm, and attention level) indicating impairment of behaviors when reduced were multiplied by -1 before calculating the sum of Z scores.

# Extraction of mtDNA

Mice were euthanized by cervical vertebral dislocation under deep anesthesia (5% isoflurane) at 6 h after surgery. The brain tissues (hippocampus, amygdala, PFC, and ACC) from both hemispheres were dissected rapidly on ice using Brain Matrices (RWD Life Science Co.) according to the maps and guides to dissection published by Paxinos and Franklin [24] and stored in liquid nitrogen. Mitochondrial samples were isolated using a Mitochondria Isolation Kit for Tissues (Beyotime, Shanghai, China) according to the manufacturer's protocol. Then, mtDNA was extracted from the pooled mitochondrial sample using a DNA isolation kit (TIANGEN, Beijing, China) with some modifications to the manufacturer's protocol. Briefly, RNaseA (100 mg/mL) and Proteinase K (50 μL/mL) was added to the enzyme mix, dounce homogenization was performed at 4 °C for 25 strokes, and samples were centrifuged at 700 × *g* at 4 °C for 5 min. Phenol-chloroform purification and ethanol precipitation were performed to increase the purity of the final mtDNA solution. The samples were verified using gel electrophoresis on 2% agarose gels and were quantified by 260 nm absorbance using a NanoDrop 2000 Spectrometer (NanoDrop Technologies, Wilmington, DE, USA).

# BamHI-HF treatment, bisulfite conversion, and sequencing

The loop of mtDNA was opened after incubation with *BamH*I-HF (New England Biolabs, Ipswich, MA, USA), which specifically recognizes GGATCC and cuts at the position of G/G. Bisulfite conversion of unmethylated cytosines to uracil in mtDNA was performed using an EZ DNA Methylation-Gold Kit (Zymo Research, Irvine, CA, USA) according to the manufacturer's protocol. The cycle conditions were 98 °C for 10 min, 64 °C for 2.5 h, and hold at 4 °C. Cleanup of bisulfite-converted DNA was performed using a spin column. Then, the bisulfite-converted DNA was amplified to obtain specific mtDNA fragments using Hot-Start Taq DNA Polymerase (Takara, Beijing, China) and specific primers. Specific primers listed in Table S1 were designed based on the *Mus musculus* mitochondrion complete genome (NCBI reference sequence: NC_005089.1). The total reaction volume was 50 μL, including 0.25 μL Ex Taq HS (5 U/μL), 5 μL Ex Taq Buffer (20 mM), 4 μL dNTP Mixture (2.5 mM each), 1 μL sense primer and anti-sense primer (1.0 μM each), 30 ng DNA template, and nuclease-free water. The cycle conditions included an initial denaturation at 95 °C for 2 min; 11 cycles of 95 °C for 20 s, 62 °C for 40 s, and 72 °C for 1 min (-0.5 °C/cycle); 24 cycles of 95 °C for 20 s, 64 °C for 30 s, and 72 °C for 1 min; and a final extension at 72 °C for 1 min. Amplified DNA products were diluted and further amplified using indexed primers. The cycle conditions were 95 °C for 2 min; 12 cycles of 95 °C for 20 s, 60 °C for 40 s, and 72 °C for 1 min; and a final extension at 72 °C for 2 min. Polymerase chain reaction (PCR) products were separated by 2%

agarose gel electrophoresis at 140 V for 35 min and purified using a Gel Extraction kit (TIANGEN). DNA Libraries were constructed, followed by sequencing on an Illumina HiSeq Xten platform according to the manufacturer's protocols. Sequencing was performed with the 2 × 150-bp paired-end mode. The basic information of 65 target CpG sites is listed in Table S2.

# Quantification of mtDNA copy number

Relative mtDNA copy numbers were quantified using real-time PCR. Total DNA was extracted from the bilateral hippocampus, amygdala, PFC, and ACC using a DNA isolation kit (TIANGEN). Real-time PCR with 25 ng DNA template, 10 μL 2 × SYBR Premix, and 0.8 μL of each 10 μM primer in a final volume of 20 μL/reaction was performed using a SYBR Premix Ex Taq II kit (Takara) on an ABI Step One Plus Real-Time PCR System (Applied Biosystems, Foster City, CA, USA) according to the manufacturer's protocol, i.e., initial denaturation at 95 °C for 10 s; 40 cycles of 95 °C for 3 s and 60 °C for 25 s; and a final dissociation step. The mitochondrial genes *ND4* and 16S rRNA were assessed in triplicate, and the nuclear housekeeping gene 18S rRNA served as a loading control. Relative mtDNA copy numbers were calculated by comparing mtDNA to 18S rRNA using the ΔΔCt method.

# Quantification of mitochondrial gene expression

Total RNA was isolated from the bilateral hippocampus, amygdala, PFC, and ACC using TRIzol reagent (Invitrogen, Carlsbad, CA, USA), and was reverse transcribed using a reverse transcription PCR kit (Takara). The expression levels of differentially methylated mitochondrial genes (*COX1*, *ND2*, and *ND5*) were determined using a SYBR Premix Ex Taq II kit (Takara) on an ABI Step One Plus Real-Time PCR System (Applied Biosystems) according to the manufacturer's protocol. The PCR conditions were as described above. Expression levels were calculated by comparing mitochondrial gene amplification levels to 18S rRNA amplification levels using the ΔΔCt method.

# Electron microscopy

After perfusion, the isolated hippocampus, amygdala, PFC, and ACC were rapidly cut into 1-mm-thick slices and fixed in 3% glutaraldehyde at 4 °C for 4 h. After washing with phosphate-buffered saline, the slices were postfixed in a solution of 1% osmium-tetroxide and 1% potassium hexacyanoferrate (II) for 1 h. Then, samples were rinsed, dehydrated in acetone, saturated, and embedded in epoxy-resin. Ultrathin slices were sectioned (64 nm) and poststained with uranyl acetate and lead citrate. Imaging was performed with a transmission electron microscope (HT7800; Hitachi Ltd., Tokyo, Japan).

# Mitochondrial isolation and western blotting

Mice were euthanized by cervical vertebral dislocation under deep anesthesia (5% isoflurane) at 6 h after surgery. The bilateral hippocampus, amygdala, PFC, and ACC were removed rapidly and stored in liquid nitrogen. Mitochondria were isolated from these tissues using a Mitochondria Isolation Kit (Beyotime) according to the manufacturer's protocol. Mitochondrial pellets were homogenized in ice-cold RIPA lysis buffer containing 50 mM Tris-HCl (pH 7.4), 150 mM NaCl, 1% Nonidet P-40, 1% sodium deoxycholate, 0.1% sodium dodecyl sulfate, and protease inhibitor tablet (Beyotime). Mitochondrial protein was

extracted, and the concentration was measured by the bicinchoninic acid method. Equivalent protein (20 μg) was separated by sodium dodecyl sulfate-polyacrylamide gel electrophoresis (10%) and transferred to polyvinylidene difluoride membranes (Millipore Corporation, Danvers, MA, USA). After blocking in 5% skim milk, the membranes were incubated with the following primary antibodies (Abcam, Cambridge, UK) overnight at 4 °C with gentle shaking: anti-DNMT1 (diluted 1:1000 in 5% w/v bovine serum albumin [BSA], 1 × TBST) and anti-voltage-dependent anion channel 1 (VDAC1; diluted 1:1000 in 5% w/v BSA, 1 × TBST). The membranes were washed, incubated with secondary antibodies conjugated with horseradish peroxidase (diluted 1:10000), and developed in enhanced chemiluminescence solution. Densities of specific bands were measured using Quantity One V4.31 analysis software (Bio-Rad, Hercules, CA, USA).

# Drug preparation and intraperitoneal injection

Resveratrol (MedChemExpress, Princeton, NJ, USA), a natural chemical activator of silent information regulator-1 (SIRT1), was dissolved in 10% dimethyl sulfoxide (DMSO) and intraperitoneally injected at a dose of 50 mg/kg body weight/day for 7 consecutive days before anesthesia and surgery. The vehicle group received an identical volume of 10% DMSO. The dose was selected in accordance with the findings of previous reports and the results of our preliminary experiments.

# Statistical analysis

Statistical analyses were performed using SPSS 20.0 (SPSS Inc., Chicago, IL, USA). Mice were assigned to different treatment groups in accordance with a random number table. Data were expressed as means ± standard deviations (SDs). Two-way repeated measures analysis of variance (ANOVA; treatment × time) was performed to determine differences in behavior tests between groups. One-way ANOVA was used to determine differences in molecular biological data. When significant main effects were observed, the sources of differences were determined by conducting Bonferroni *post-hoc* tests. Results with *P* values of less than 0.05 were considered statistically significant.

## Results

# Anesthesia- and surgery-induced time-dependent delirium-like behaviors in young and old mice

In buried food tests, anesthesia and surgery increased the latency to eat food in 6-month-old mice compared with that in age-matched control mice at 9 h after surgery ($P < 0.05$; Fig. 1a). In addition, compared with age-matched control mice, the latency to eat food was also increased in 18-month-old mice at 6, 9, and 24 h after surgery ($P < 0.05$; Fig. 1i). These data suggested that anesthesia and surgery could impair attention, organized thinking, and consciousness, which are necessary for finding and eating food.

In open field tests, anesthesia and surgery did not alter the total distance in 6- or 18-month-old mice compared with that in age-matched control mice at 6, 9, or 24 h after surgery (Supplemental Information Fig. S1). Anesthesia and surgery decreased the time spent in the center and the freezing time of 6-month-old mice compared with that of age-matched control mice at 6 h after surgery, but did not change the latency to center in 6-month-old mice ($P < 0.05$; Fig. 1b, c). In addition, compared with age-matched control mice, the time spent in the center in 18-month-old mice was decreased, and the latency to center in 18-month-old mice was increased at 6 and 9 h after surgery. Moreover, the freezing time in 18-month-old mice was decreased at all time points after surgery ($P < 0.05$; Fig. 1j–l). These data suggested that anesthesia and surgery could induce anxiety-like behaviors and impair exploratory behaviors and awareness of the environment without affecting locomotor activity in mice.

In Y maze tests, compared with age-matched control mice, the number of entries into the novel arm was decreased in 6-month-old mice at 9 h after surgery, and the duration in the novel arm was decreased in 6-month-old mice at 6 h after surgery ($P < 0.05$; Fig. 1e, f). In addition, anesthesia and surgery decreased the number of entries into the novel arm in 18-month-old mice compared with that in age-matched control mice at 6 and 9 h after surgery and decreased the duration in the novel arm for 18-month-old mice at 6 h after surgery ($P < 0.05$; Fig. 1m, n). These data suggested that anesthesia and surgery could impair the spatial memory of mice.

In NNATs, anesthesia and surgery did not alter the attention levels of 6-month-old mice compared with age-matched control mice at 6, 9, or 24 h after surgery ($P > 0.05$; Fig. 1g). However, compared with age-matched control mice, the attention levels of 18-month-old mice were decreased at 24 h after surgery ($P < 0.05$; Fig. 1o).

The mean composite Z score for 6-month-old mice in the surgery group was significantly higher than that in the age-matched control group at 6 and 9 h, but not 24 h after surgery (Fig. 1h). In 18-month-old mice, the mean composite Z score in the surgery group was significantly greater than that in the control group at all time points after surgery (Fig. 1p). Collectively, these data suggested that abdominal surgery under isoflurane anesthesia could induce time-dependent postoperative delirium, manifested as impairment of certain natural and learned behaviors both in young and old mice; this effect was more profound in old mice.

# SIRT1 activation by resveratrol ameliorated anesthesia- and surgery-induced delirium-like behaviors

Given previous findings showing that energy deficits, oxidative stress, and neuroinflammation associated with mitochondrial dysfunction may contribute to the mechanism of POD [8], and because SIRT1 is a key modulator of mitochondrial homeostasis [25], we employed resveratrol to determine whether SIRT1 activation could ameliorate anesthesia- and surgery-induced delirium-like behaviors in 18-month-old mice. Buried food tests showed that resveratrol ameliorated anesthesia- and surgery-induced increases in the latency to eat food at 6, 9, and 24 h after surgery compared with that in mice treated with vehicle ($P < 0.05$; Fig. 2a). In open field tests, resveratrol ameliorated anesthesia- and surgery-induced decreases in

the time spent in the center and in the freezing time at 6 and 9 h after surgery and ameliorated the increase in latency to center at 9 h after surgery compared with that in mice treated with vehicle ($P < 0.05$; Fig. 2b–d). Resveratrol also ameliorated anesthesia- and surgery-induced reductions in the number of entries into the novel arm in Y maze tests at 9 h after surgery ($P < 0.05$; Fig. 2e). However, resveratrol did not affect the decrease in the duration in the novel arm induced by anesthesia and surgery in Y maze tests or the decrease in attention levels induced by anesthesia and surgery in NNATs during the observation period ($P > 0.05$; Fig. 2f, g). The increase in the mean composite Z score induced by anesthesia and surgery was significantly decreased in mice treated with resveratrol at 6 and 9 h after surgery (Fig. 2h). Collectively, these data suggested that SIRT1 activation by resveratrol could ameliorate anesthesia- and surgery-induced delirium-like behaviors.

*Anesthesia and surgery altered mtDNA methylation levels in different brain regions in young and old mice*

To investigate the effects of anesthesia and surgery on mtDNA methylation, we evaluated 5-mC methylation at 60 CpG sites of specific gene loci and at 5 CpG sites of the D-loop at 6 h after surgery. Consistent with previous reports, the average methylation levels of different CpG sites were all less than 3% and showed regional differences across the mitochondrial genome. Several CpG sites exhibited significantly different levels of mtDNA methylation among groups (Fig. 3).

In the hippocampus, there were five sites located within the 12S rRNA region (318, 355, 362), *ND1* region (2851), and *COX1* region (6640) that showed lower levels of methylation and three sites located within the *COX3* region (8845), *ND4* region (10599), and D-loop region (15856) that showed higher levels of methylation after surgery in 6-month-old mice compared with that in age-matched control mice. In 18-month-old mice, there were four sites located within the *ND2* region (4136), *COX1* region (6640), and *ND5* region (13119, 13242) that showed lower levels of methylation and one site located within the D-loop region (15856) that showed higher levels of methylation in the hippocampus after surgery compared with that in age-matched control mice. In addition, resveratrol reversed anesthesia- and surgery-induced changes in methylation levels at site 6640 within the *COX1* region and at site 15856 within the D-loop region, i.e., the two differential methylation sites identified both in 6- and 18-month-old mice undergoing surgery (Table 1).

Table 1
Differential methylation of CpG sites in hippocampus of control and surgery mice at different ages

| CpG site | Annotation | Control (n = 9) vs Surgery (n = 11) (6 months) | | Control (n = 10) vs Surgery (n = 11) (18 months) | | Surgery + Resveratrol (n = 10) vs Surgery + Vehicle (n = 10) | |
|---|---|---|---|---|---|---|---|
| | | p | Difference | p | Difference | p | Difference |
| 230 | 12S rRNA | | | | | 0.018 | 0.950 |
| 318 | 12S rRNA | 0.02 | -0.367 | | | | |
| 355 | 12S rRNA | 0.04 | -0.627 | | | | |
| 362 | 12S rRNA | 0.001 | -1.016 | | | | |
| 2851 | ND1 | 0.009 | -0.311 | | | | |
| 2904 | ND1 | | | | | 0.037 | 0.172 |
| 4136 | ND2 | | | 0.031 | -0.232 | 0.041 | 0.085 |
| 6640 | COX1 | 0.007 | -0.201 | 0.039 | -0.322 | 0.011 | -0.239 |
| 7337 | COX2 | | | | | 0.022 | 0.091 |
| 8845 | COX3 | 0.023 | 0.204 | | | 0.045 | 0.161 |
| 10599 | ND4 | 0.02 | 0.197 | | | 0.009 | 0.122 |
| 13119 | ND5 | | | 0.028 | -0.264 | 0.049 | 0.125 |
| 13242 | ND5 | | | 0.022 | -0.140 | | |
| 15856 | D-loop | < 0.001 | 0.642 | 0.002 | 0.511 | < 0.001 | 0.482 |
| Data were analyzed by one-way ANOVA. | | | | | | | |

In the PFC, there were four sites located within *ND2* region (4094), *ATP6* region (8048), and *ND4L* region (10075, 10084) that showed lower levels of methylation after surgery in 6-month-old mice compared with that in age-matched control mice. In 18-month-old mice, there were nine sites located within the 12S rRNA region (264, 320, 352), 16S rRNA region (1333), *ND2* region (4136), *COX1* region (6640), *ND3* region (9582), *ND4L* region (10144), and *ND4* region (10632) that showed lower levels of methylation and three sites located within the *ND5* region (13119) and D-loop region (15833, 15856) that showed higher levels of methylation in the PFC after surgery compared with that in age-matched control mice. In addition, resveratrol reversed anesthesia- and surgery-induced changes in methylation levels at site 4136 within the *ND2* region, site 6640 within the *COX1* region, and site 15856 within the D-loop region, i.e., the three differential methylation sites identified in 18-month-old mice undergoing surgery (Table 2).

Table 2
Differential methylation of CpG sites in prefrontal cortex of control and surgery mice at different ages

| CpG site | Annotation | Control (n = 5) vs Surgery (n = 6) (6 months) | | Control (n = 5) vs Surgery (n = 5) (18 months) | | Surgery + Resveratrol (n = 7) vs Surgery + Vehicle (n = 6) | |
|---|---|---|---|---|---|---|---|
| | | p | Difference | p | Difference | p | Difference |
| 264 | 12S rRNA | | | 0.031 | -0.861 | | |
| 320 | 12S rRNA | | | 0.029 | -1.301 | | |
| 352 | 12S rRNA | | | 0.026 | -1.127 | | |
| 1333 | 16S rRNA | | | 0.002 | -0.420 | | |
| 4094 | ND2 | 0.016 | -0.230 | | | | |
| 4136 | ND2 | | | 0.040 | -0.194 | 0.046 | -0.417 |
| 6640 | COX1 | | | 0.045 | -0.152 | 0.037 | -0.348 |
| 7434 | COX2 | | | | | 0.019 | -0.183 |
| 8048 | ATP6 | 0.015 | -0.294 | | | | |
| 9582 | ND3 | | | < 0.001 | -0.152 | | |
| 10075 | ND4L | 0.025 | -0.277 | | | | |
| 10084 | ND4L | 0.001 | -0.249 | | | | |
| 10144 | ND4L | | | 0.016 | -0.227 | | |
| 10632 | ND4 | | | 0.013 | -0.318 | | |
| 13119 | ND5 | | | 0.015 | 0.649 | 0.044 | -0.139 |
| 15833 | D-loop | | | 0.011 | 0.767 | | |
| 15856 | D-loop | | | 0.015 | 0.866 | 0.003 | 0.920 |
| Data were analyzed by one-way ANOVA. | | | | | | | |

In the amygdala and ACC, fewer sites showed significant differences in mtDNA methylation levels. In ACC, the methylation levels were decreased at site 7413 within the *COX2* region and increased at site 8868 within the *COX3* region after surgery in 6-month-old mice compared with that in age-matched control mice. In 18-month-old mice, the methylation levels were decreased at site 230 within the 12S rRNA region, site 4136 within the *ND2* region, and site 8848 within the *COX3* region and increased at site 7984 within the *ATP6* region after surgery in 18-month-old mice compared with that in age-matched control mice (Table 3). In the amygdala, methylation levels were decreased at site 6570 within the *COX1* region

and site 2880 within the *ND1* region and increased at site 6643 within the *COX1* region and site 10599 within the *ND4* region after surgery compared with that in age-matched control mice (Table 4). Resveratrol changed the methylation levels at site 10591 within the *ND4* region and site 14979 within the *CYTB* region in the ACC and site 2935 within the *ND1* region, site 7487 within the *COX2* region, and site 8123 within the *ATP6* region in the amygdala.

Table 3
Differential methylation of CpG sites in anterior cingulate cortex of control and surgery mice at different ages

| CpG site | Annotation | Control (n = 5) vs Surgery (n = 5) (6 months) | | Control (n = 5) vs Surgery (n = 7) (18 months) | | Surgery + Resveratrol (n = 8) vs Surgery + Vehicle (n = 5) | |
|---|---|---|---|---|---|---|---|
| | | p | Difference | p | Difference | p | Difference |
| 230 | 12S rRNA | | | 0.018 | -0.961 | | |
| 4136 | ND2 | | | 0.004 | -0.181 | | |
| 7413 | COX2 | 0.032 | -0.317 | | | | |
| 7984 | ATP6 | | | 0.041 | 0.229 | | |
| 8868 | COX3 | 0.019 | 0.264 | 0.037 | -0.256 | | |
| 10591 | ND4 | | | | | 0.006 | -0.143 |
| 14979 | CYTB | | | | | 0.046 | -0.100 |
| Data were analyzed by one-way ANOVA. | | | | | | | |

Table 4
Differential methylation of CpG sites in amygdala of control and surgery mice at different ages

| CpG site | Annotation | Control (n = 7) vs Surgery (n = 7) (6 months) | | Control (n = 8) vs Surgery (n = 5) (18 months) | | Surgery + Resveratrol (n = 5) vs Surgery + Vehicle (n = 9) | |
|---|---|---|---|---|---|---|---|
| | | p | Difference | p | Difference | p | Difference |
| 2880 | ND1 | | | 0.045 | -0.164 | | |
| 2935 | ND1 | | | | | < 0.001 | 0.276 |
| 6570 | COX1 | 0.042 | -0.184 | | | | |
| 6643 | COX1 | 0.007 | 0.208 | | | | |
| 7487 | COX2 | | | | | 0.028 | 0.230 |
| 8123 | ATP6 | | | | | 0.026 | -0.144 |
| 10599 | ND4 | | | 0.040 | 0.131 | | |
| Data were analyzed by one-way ANOVA. | | | | | | | |

# Anesthesia and surgery altered mtDNA copy numbers, gene expression, and morphology

Because mtDNA methylation may regulate mitochondrial biogenesis, mtDNA replication, and transcription, we next evaluated relative copy numbers of mtDNA expressed as a ratio of *ND4* and 16S rRNA gene copies to 18S rRNA gene copies at 6 h after surgery using RT-PCR. mtDNA copy numbers were significantly decreased in the hippocampus and PFC after surgery in both 6- and 18-month-old mice compared with that in age-matched control mice. Resveratrol reversed anesthesia- and surgery-induced decreases in mtDNA copy numbers in the hippocampus and PFC compared with that in vehicle-treated mice. However, no significant differences in mtDNA copy numbers were found in the amygdala or ACC (Fig. 4).

To further clarify the downstream effects of mtDNA methylation on mtDNA transcription, RT-PCR was used to measure the expression levels of differentially methylated mitochondrial genes (*COX1*, *ND2*, and *ND5*). Our results showed that anesthesia and surgery induced greater changes in mitochondrial gene expression in 18-month-old mice than in 6-month-old mice. In 18-month-old mice, *COX1* gene expression was increased, whereas *ND2* and *ND5* gene expression was decreased significantly in both the hippocampus and PFC at 6 h after surgery compared with that in control mice. Resveratrol ameliorated anesthesia- and surgery-induced changes in such gene expression in the hippocampus and PFC compared with that in vehicle-treated mice. However, no significant differences in gene expression were found in the amygdala or ACC (Fig. 5).

To assess whether mtDNA methylation affected mitochondrial morphology, which is critical for maintaining mitochondrial function, we performed electron microscopy studies to observe the ultrastructure of mitochondria in different brain regions at 6 h after surgery. There were more round and damaged mitochondria, manifested as an unclear structure, distorted cristae, and swelling of mitochondria in both the hippocampus and PFC after surgery compared with that in age-matched control mice. Resveratrol ameliorated anesthesia- and surgery-induced changes in mitochondrial morphology compared with that in vehicle-treated mice (Fig. 6).

# Anesthesia and surgery altered the expression of DNA methyltransferase in mitochondria

Western blotting results using purified mitochondrial fractions showed that the expression levels of DNMT1 were significantly increased in the hippocampus and PFC of 18-month-old mice at 6 h after surgery compared with that in age-matched control mice. In 6-month-old mice, anesthesia- and surgery-induced upregulation of DNMT1 was observed only in PFC. Resveratrol increased the expression levels of DNMT1 in the PFC compared with that in vehicle-treated mice (Fig. 7).

# Discussion

In the current study, we examined methylation levels at 65 CpG sites in the mitochondrial genome in a mouse model of POD. We found that laparotomy under isoflurane anesthesia induced acute postoperative impairment of natural and learned behaviors, including inattention, disorganized thinking, altered levels of consciousness, and memory decline in an age-dependent manner. Moreover, mtDNA methylation drift manifested as an increase in methylation levels in the D-loop and an increase or decrease in methylation levels at several coding gene loci, ultimately resulting in reduced mtDNA copy numbers, altered mitochondrial gene expression, and damaged mitochondrial structures in the hippocampus and PFC after surgery; this could be the important epigenetic mechanism of delirium-like behaviors. We also showed that SIRT1 activation ameliorated anesthesia- and surgery-induced mitochondrial dysfunction and delirium-like behaviors by regulating mitochondrial DNA methyltransferase-mediated mtDNA methylation. Our findings provided evidence to establish the relationship between mtDNA epigenetic mechanisms and POD.

Mitochondria, which synthesize ATP and supply cellular energy through the respiration chain and oxidative phosphorylation system, play essential roles in maintaining neuronal functions. Mitochondrial impairment and dysfunction lead to ROS production, energy deficits, and neuroinflammation in the brain, representing the key feature of POD [8, 26, 27]. Recently, mtDNA methylation, which regulates mtDNA gene expression and replication and thus directly affects the structure and function of mitochondrion, has been proposed as a cause of ageing and many neurodegenerative diseases and may be a valuable epigenetic marker and therapeutic target [17–20, 28]. Illumina sequencing of 82 human blood samples indicated that the methylation levels at 54 CpG sites in the mitochondrial genome varied according to age and that hypomethylation of two of these CpG sites was significantly correlated with chronological age

[20]. A dynamic pattern including both increases and decreases in methylation levels at various sites of mtDNA in human and mouse brains, i.e., the mtDNA methylation drift, contributes to the pathogenic mechanisms of Alzheimer's disease and Parkinson's disease [17, 18]. Our data provided further evidence regarding mtDNA methylation drift, suggesting mtDNA epigenetic modulation in POD.

Several differential methylation sites of the D-loop and specific coding gene loci in mtDNA were identified in young and old mice exhibiting postoperative delirium-like behaviors compared with those in age-matched control mice in the current study. The D-loop, an important noncoding region of mtDNA, contains promoters for both the heavy and light strands of mitochondrial genes and controls mitochondrial genome replication and transcription [28]. The association of the hypermethylated D-loop with decreased mtDNA copy numbers was also reported in insulin resistance and Alzheimer's disease [17, 30]. In contrast, some studies have observed hypomethylation of the D-loop region with decreased mtDNA copy numbers in brain samples from patients with Alzheimer's disease, suggesting that other cofounding factors may participate in D-loop methylation-regulated mitochondrial genome replication [18]. In this study, we showed that anesthesia and surgery induced significant hypermethylation in the D-loop, resulting in decreased mtDNA copy numbers in the hippocampus and PFC of 6- and 18-month-old mice. Theoretically, for specific coding genes, mtDNA methylation levels negatively correlate with mitochondrial gene transcript abundance. However, mtDNA methylation drift with decreased methylation levels at most coding gene loci was observed in brains from older humans, and mitochondrial gene expression decreased with age [13]. Our data suggested that anesthesia and surgery induced mtDNA methylation drift at coding gene loci, thereby influencing the transcriptional levels of *COX1*, *ND2*, and *ND5*, which encode the subunits of cytochrome c oxidase (complex IV) and NADH dehydrogenase (complex I) in the hippocampus and PFC of 6- and 18-month-old mice. We speculated that hypomethylation at most coding genes, which could promote transcription regulated by the hypermethylation of D-loop, may represent an interrelated compensatory mechanism [17]. The decreased mtDNA copy number and abnormal transcript abundance of coding genes, resulting in damage to mitochondrial structure and function after surgery in the hippocampus and PFC, may be the underlying mechanism of POD.

The methylation of mtDNA is regulated by DNMT1, which translocates to the mitochondria via a mitochondrial targeting sequence [14]. Previous studies have suggested that age-related oxidative stress and inflammatory conditions downregulate the expression and function of DNMTs [31]. Our data suggested that anesthesia and surgery increased the expression levels of DNMT1 in the mitochondria, resulting in mtDNA methylation drift, i.e., global hypomethylation and regional hypermethylation in the hippocampus and PFC of 6- and 18-month-old mice. SIRT1, an NAD+-dependent histone deacetylase, exerts various beneficial effects, such as suppression of the physiological signs of aging via regulation of the expression, acetylation, and activity of DNMTs [31]. Resveratrol, which activates SIRT1 through allosteric interaction and increases SIRT1 affinity for both NAD + and the acetylated substrate, not only regulates the expression and acetylation of DNMT1 directly but also modulates the binding of DNMT1 and the mitochondrial genome indirectly via regulating peroxisome proliferator-activated receptor gamma coactivator 1α and nuclear respiratory factor 1, which interact with DNMT1 [14, 31]. Our data suggested that resveratrol regulated the expression of DNMT1 and thus ameliorated anesthesia- and surgery-

induced mtDNA methylation drift, mitochondrial dysfunction, and delirium-like behaviors. Notably, resveratrol only perturbed mtDNA methylation levels regionally, not globally.

There were several limitations to the current study. First, our analysis of mtDNA methylation was limited to 5-mC levels at CpG sites of the mitochondrial genome. However, 5-hmC is also present in the mitochondrial genome, and non-CpG sites in mitochondria can also be methylated [13]. Further studies are needed to identify 5-hmC levels and methylation profiles at non-CpG sites in mitochondria in POD. Another important concept is the mechanism of upregulation of DNMT1-mediated mtDNA global hypomethylation and regional hypermethylation. Finally, the regulatory mechanism of SIRT1 still remains elusive. In addition to alterations in DNMT1 expression and activity, activated SIRT1 interacts with various substrates and exerts multiple protective effects, which can influence mtDNA methylation levels directly or indirectly [32] and should also be taken into account.

# Conclusions

In conclusion, mtDNA methylation drift presented as global hypomethylation and regional hypermethylation in the hippocampus and PFC, mediated impairment of mitochondrial structure and function, and played key roles in POD. These data supported the existence of epigenetic mtDNA regulation in POD. However, further research is required to explore the associated mechanisms.

# Abbreviations

5-mC
5-methylcytosine; ACC:anterior cingulate cortex; CAM:Confusion Assessment Method; COX:cytochrome oxidase; Cyt b:cytochrome b; D-loop:displacement loop; DNMT1:DNA methyltransferase 1; mtDNA:mitochondrial DNA; MTS:mitochondrial targeting sequence; ND:NADH dehydrogenase subunits; NNAT:non‐selective non‐sustained attention test; PFC:prefrontal cortex; POD:postoperative delirium; ROS:reactive oxygen species; SIRT1:Silent information regulator-1; tRNAs:transfer RNAs; rRNAs:ribosomal RNAs.

# Declarations

### Ethics approval and consent to participate

Ethics approval was obtained from the Institutional Animal Care and Use Committee of Nanjing University. All applicable institutional and/or national guidelines for the care and use of animals were followed.

### Consent for publication

Not applicable.

### Availability of data and materials

The data, analytic methods, and study materials are included in this published article and its supplementary information files. All sequencing documents in this study are available from the corresponding author on reasonable request.

### Competing interests

The authors declare no competing interests.


### Funding

This work was supported by the National Natural Science Foundation of China (grant nos. 81771142 and 81971044), Project of Jiangsu Provincial Six Talent Peaks (grant no. YY-084), and Promotion Project for Youth Talent in Science and Technology from the Association of Science and Technology in Jiangsu Province.


### Authors' contributions

YL and ZLM conceived and designed the experiments; YL and SY carried out most of the experiments and analyzed the data; WZ, YY and MJ assisted in experiments; YL and ZLM wrote the manuscript; ZLM and XPG supervised the study. All authors read and approved the final manuscript.


### Acknowledgments

Not applicable.


### Authors' information (optional)

Not applicable.

## References


1. Whitlock EL, Vannucci A, Avidan MS. Postoperative delirium. Minerva Anestesiol. 2011;77:448–56.
2. Sturm H, Wildermuth R, Stolz R, Bertram L, Eschweiler GW, Thomas C, Rapp M, Joos S. Diverging awareness of postoperative delirium and cognitive dysfunction in German health care providers. Clin Interv Aging. 2019;14:2125–35.
3. Ansaloni L, Catena F, Chattat R, Fortuna D, Franceschi C, Mascitti P, Melotti RM. Risk factors and incidence of postoperative delirium in elderly patients after elective and emergency surgery. Br J Surg. 2010;97:273–80.
4. Vasilevskis EE, Han JH, Hughes CG, Ely EW. Epidemiology and risk factors for delirium across hospital settings. Best Pract Res Clin Anaesthesiol. 2012;26:277–87.
5. Inouye SK, Westendorp RG, Saczynski JS. Delirium in elderly people. Lancet. 2014;383:911–22.

6. Saczynski JS, Marcantonio ER, Quach L, Fong TG, Gross A, Inouye SK, Jones RN. Cognitive trajectories after postoperative delirium. N Engl J Med. 2012;367:30–9.
7. Inouye SK, van Dyck CH, Alessi CA, Balkin S, Siegal AP, Horwitz RI. Clarifying confusion: the confusion assessment method. A new method for detection of delirium. Ann Intern Med. 1990;113:941–8.
8. Peng M, Zhang C, Dong Y, Zhang Y, Nakazawa H, Kaneki M, Zheng H, Shen Y, Marcantonio ER, Xie Z. Battery of behavioral tests in mice to study postoperative delirium. Sci Rep. 2016;6:29874.
9. Anderson S, Bankier AT, Barrell BG, de Bruijn MH, Coulson AR, Drouin J, Eperon IC, Nierlich DP, Roe BA, Sanger F, Schreier PH, Smith AJ, Staden R, Young IG. Sequence and organization of the human mitochondrial genome. Nature. 1981;290:457–65.
10. Asin-Cayuela J, Gustafsson CM. Mitochondrial transcription and its regulation in mammalian cells. Trends Biochem Sci. 2007;32:111–7.
11. Lee SR, Han J. Mitochondrial nucleoid: shield and switch of the mitochondrial genome. Oxid Med Cell Longev. 2017;2017:8060949.
12. Byun HM, Panni T, Motta V, Hou L, Nordio F, Apostoli P, Bertazzi PA, Baccarelli AA. Effects of airborne pollutants on mitochondrial DNA methylation. Part Fibre Toxicol. 2013;10:18.
13. Dou X, Boyd-Kirkup JD, McDermott J, Zhang X, Li F, Rong B, Zhang R, Miao B, Chen P, Cheng H, Xue J, Bennett D, Wong J, Lan F, Han JJ. The strand-biased mitochondrial DNA methylome and its regulation by DNMT3A. Genome Res. 2019;29:1622–34.
14. Shock LS, Thakkar PV, Peterson EJ, Moran RG, Taylor SM. DNA methyltransferase 1, cytosine methylation, and cytosine hydroxymethylation in mammalian mitochondria. Proc Natl Acad Sci USA. 2011;108:3630–5.
15. D'Aquila P, Montesanto A, Guarasci F, Passarino G, Bellizzi D. Mitochondrial genome and epigenome: two sides of the same coin. Front Biosci. 2017;22:888–908.
16. Tsai TS, St John JC. The effects of mitochondrial DNA supplementation at the time of fertilization on the gene expression profiles of porcine preimplantation embryos. Mol Reprod Dev. 2018;85:490–504.
17. Blanch M, Mosquera JL, Ansoleaga B, Ferrer I, Barrachina M. Altered mitochondrial DNA methylation pattern in Alzheimer disease-related pathology and in Parkinson disease. Am J Pathol. 2016;186:385–97.
18. Xu Y, Xu L, Han M, Liu X, Li F, Zhou X, Wang Y, Bi J. Altered mitochondrial DNA methylation and mitochondrial DNA copy number in an APP/PS1 transgenic mouse model of Alzheimer disease. Biochem Biophys Res Commun. 2019;520:41–6.
19. Mishra M, Kowluru RA. Epigenetic modification of mitochondrial DNA in the development of diabetic retinopathy. Investig Ophthalmol Vis Sci. 2015;56:5133–42.
20. Mawlood SK, Dennany L, Watson N, Dempster J, Pickard BS. Quantification of global mitochondrial DNA methylation levels and inverse correlation with age at two CpG sites. Aging. 2016;8:636–41.

21. Lazarini F, Gabellec MM, Torquet N, Lledo PM. Early activation of microglia triggers long-lasting impairment of adult neurogenesis in the olfactory bulb. J Neurosci. 2012;32:3652–64.
22. Millecamps M, Etienne M, Jourdan D, Eschalier A, Ardid D. Decrease in non-selective, non-sustained attention induced by a chronic visceral inflammatory state as a new pain evaluation in rats. Pain. 2004;109:214–24.
23. Moller JT, Cluitmans P, Rasmussen LS, Houx P, Rasmussen H, Canet J, Rabbitt P, Jolles J, Larsen K, Hanning CD, Langeron O, Johnson T, Lauven PM, Kristensen PA, Biedler A, van Beem H, Fraidakis O, Silverstein JH, Beneken JE, Gravenstein JS. Long-term postoperative cognitive dysfunction in the elderly ISPOCD1 study, ISPOCD investigators. International Study of Post-Operative Cognitive Dysfunction. Lancet. 1998;351:857–61.
24. Paxinos G, Franklin KBJ. The Mouse Brain in Stereotaxic Coordinates. 4th Ed. Academic Press; 2012.
25. Katsyuba E, Mottis A, Zietak M, De Franco F, van der Velpen V, Gariani K, Ryu D, Cialabrini L, Matilainen O, Liscio P, Giacchè N, Stokar-Regenscheit N, Legouis D, de Seigneux S, Ivanisevic J, Raffaelli N, Schoonjans K, Pellicciari R, Auwerx J. De novo NAD + synthesis enhances mitochondrial function and improves health. Nature. 2018;563:354–9.
26. Lu Y, Chen L, Ye J, Chen C, Zhou Y, Li K, Zhang Z, Peng M. Surgery/Anesthesia disturbs mitochondrial fission/fusion dynamics in the brain of aged mice with postoperative delirium. Aging. 2020;12:844–64.
27. Liufu N, Liu L, Shen S, Jiang Z, Dong Y, Wang Y, Culley D, Crosby G, Cao M, Shen Y, Marcantonio E, Xie Z, Zhang Y. Anesthesia and surgery induce age-dependent changes in behaviors and microbiota. Aging. 2020;12:1965–85.
28. Stoccoro A, Siciliano G, Migliore L, Coppede F. Decreased methylation of the mitochondrial D-loop region in late-onset Alzheimer's disease. J Alzheimers Dis. 2017;59:559–64.
29. Bellizzi D, D'Aquila P, Scafone T, Giordano M, Riso V, Riccio A, Passarino G. The control region of mitochondrial DNA shows an unusual CpG and non-CpG methylation pattern. DNA Res. 2013;20:537–47.
30. Zheng LD, Linarelli LE, Liu L, Wall SS, Greenawald MH, Seidel RW, Estabrooks PA, Almeida FA, Cheng Z. Insulin resistance is associated with epigenetic and genetic regulation of mitochondrial DNA in obese humans. Clin Epigenet. 2015;7:60.
31. Maugeri A, Barchitta M, Mazzone MG, Giuliano F, Basile G, Agodi A. Resveratrol modulates SIRT1 and DNMT functions and restores LINE-1 methylation levels in ARPE-19 cells under oxidative stress and inflammation. Int J Mol Sci. 2018;19:2118.
32. Liu Y, Ni Y, Zhang W, Sun YE, Jiang M, Gu WJ, Ma ZL, Gu XP. Anti-nociceptive effects of caloric restriction on neuropathic pain in rats involves silent information regulator 1. Br J Aneasth. 2018;120:807–17.

# Figures

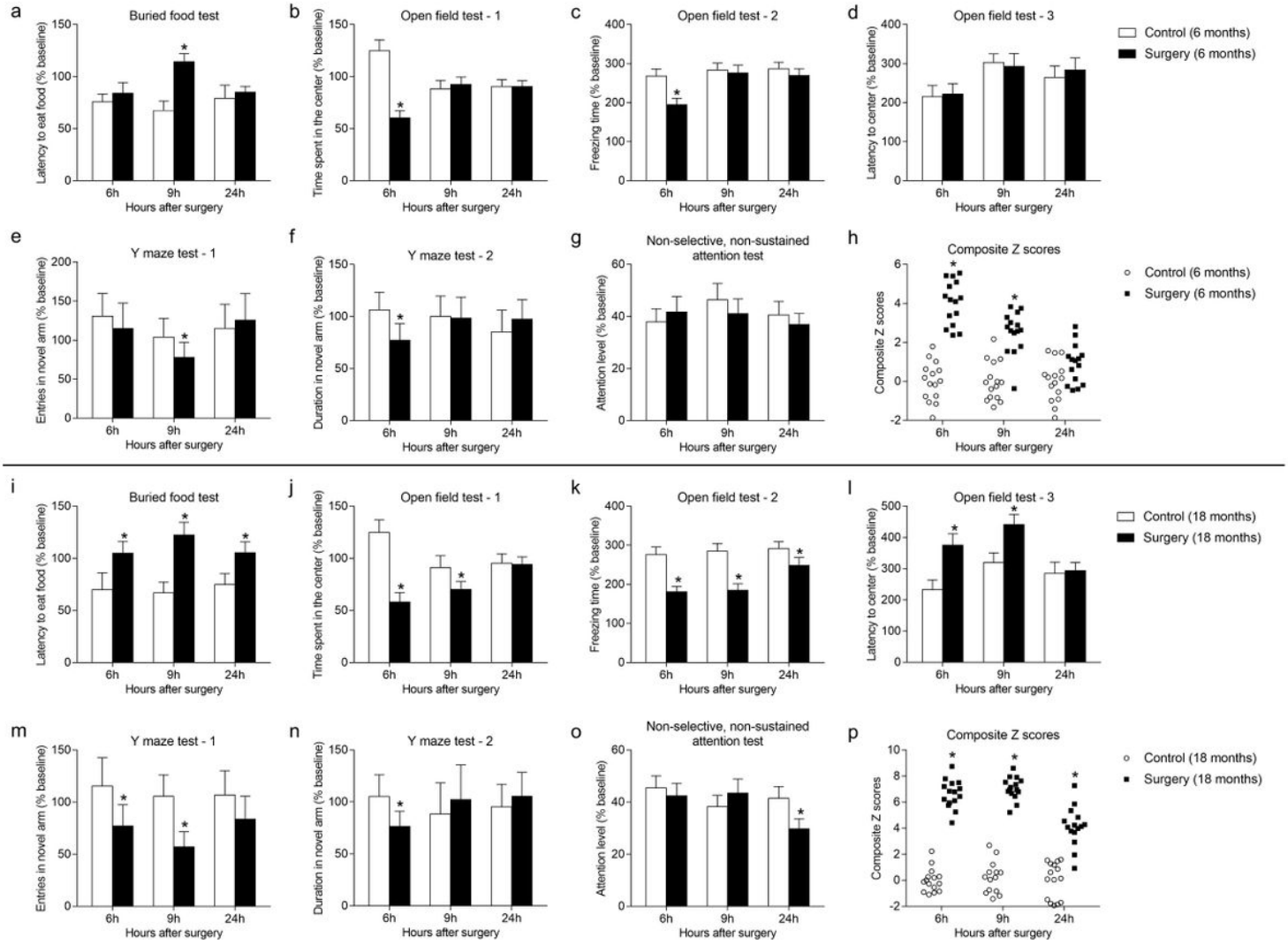


## Figure 1

Anesthesia and surgery induced time-dependent delirium-like behaviors in young and old mice. (a) Buried food tests, (b–d) open field tests (time spent in the center, freezing time, latency to center), (e, f) Y maze tests (entries in the novel arm, duration in the novel arm), and (g) nonselective, nonsustained attention tests (n = 15) were monitored in 6-month-old mice at 6, 9, and 24 h after anesthesia and surgery. (i) Buried food tests, (j–l) open field tests (time spent in the center, freezing time, latency to center), (m, n) Y maze tests (entries in the novel arm, duration in the novel arm), and (o) nonselective, nonsustained attention tests (n = 15) were monitored in 18-month-old mice at 6, 9, and 24 h after anesthesia and surgery. (h, p) Composite Z scores in 6- or 18-month-old mice quantitatively demonstrated the postoperative delirium-like behaviors in the control and surgery groups. Data are means ± SDs and were analyzed by two-way repeated measures ANOVA. *, $P < 0.05$.

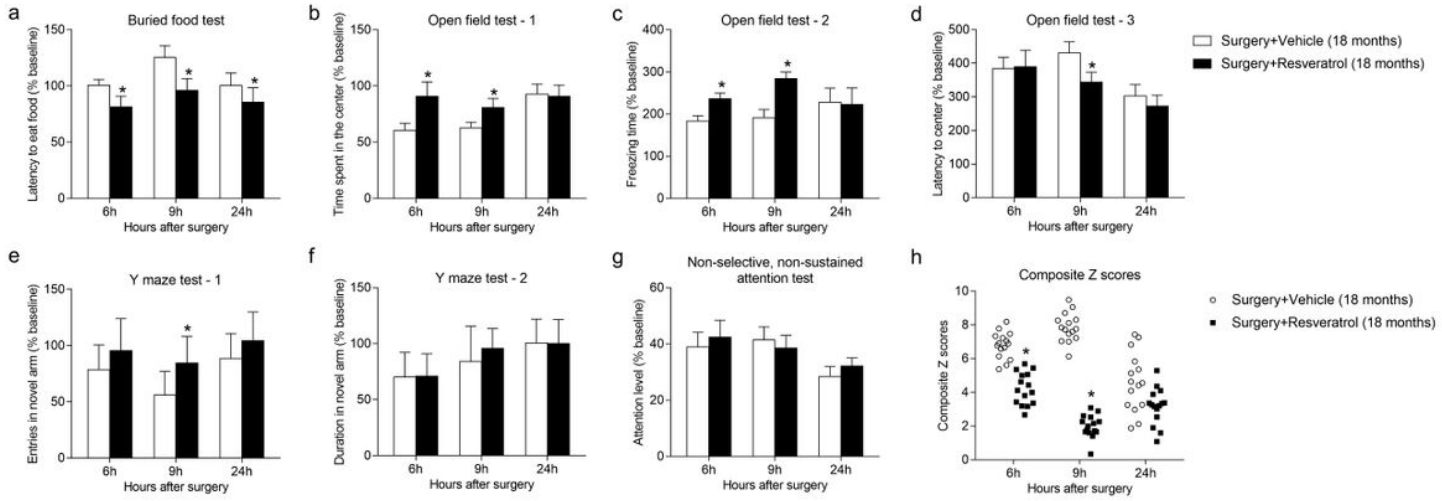


## Figure 2

Intraperitoneal injection of resveratrol ameliorated anesthesia- and surgery-induced delirium-like behaviors in 18-month-old mice. (a) Buried food tests, (b–d) open field tests (time spent in the center, freezing time, latency to center), (e, f) Y maze tests (entries in the novel arm, duration in the novel arm), and (g) nonselective, nonsustained attention tests (n = 15) were monitored at 6, 9, and 24 h after anesthesia and surgery. (h) Composite Z scores quantitatively demonstrated that pretreatment with resveratrol ameliorated postoperative delirium-like behaviors in 18-month-old mice. Data are means ± SDs and were analyzed by two-way repeated measures ANOVA. *, P < 0.05.

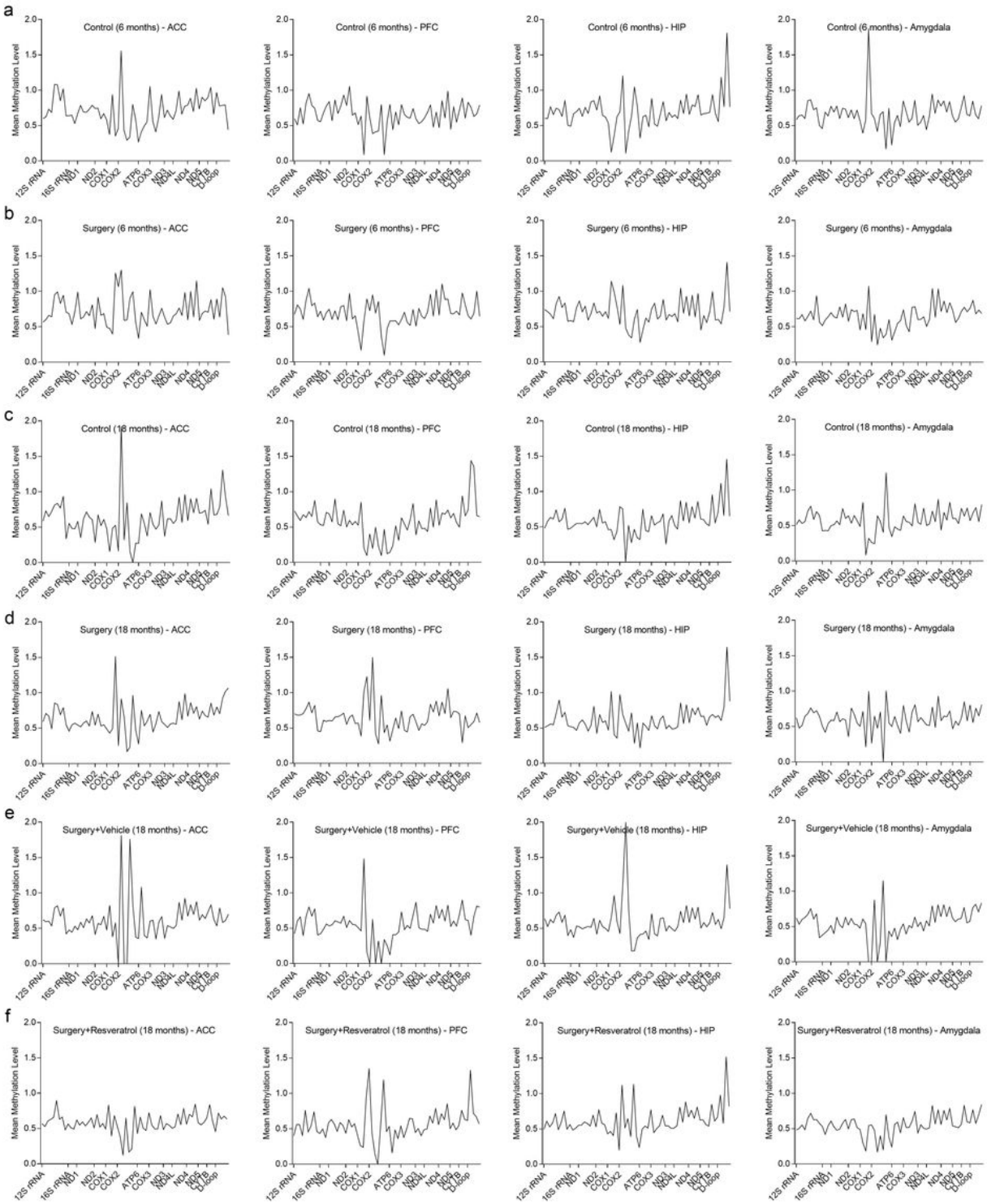


## Figure 3

Mean methylation levels at 65 CpG sites across the mitochondrial genome in the hippocampus, prefrontal cortex, amygdala, and anterior cingulate cortex of 6-month-old mice in (a) the control group and (b) surgery group and of 18-month-old mice in (c) the control group, (d) surgery group, (e) surgery + vehicle group, and (f) surgery + resveratrol group at 6 h after surgery.

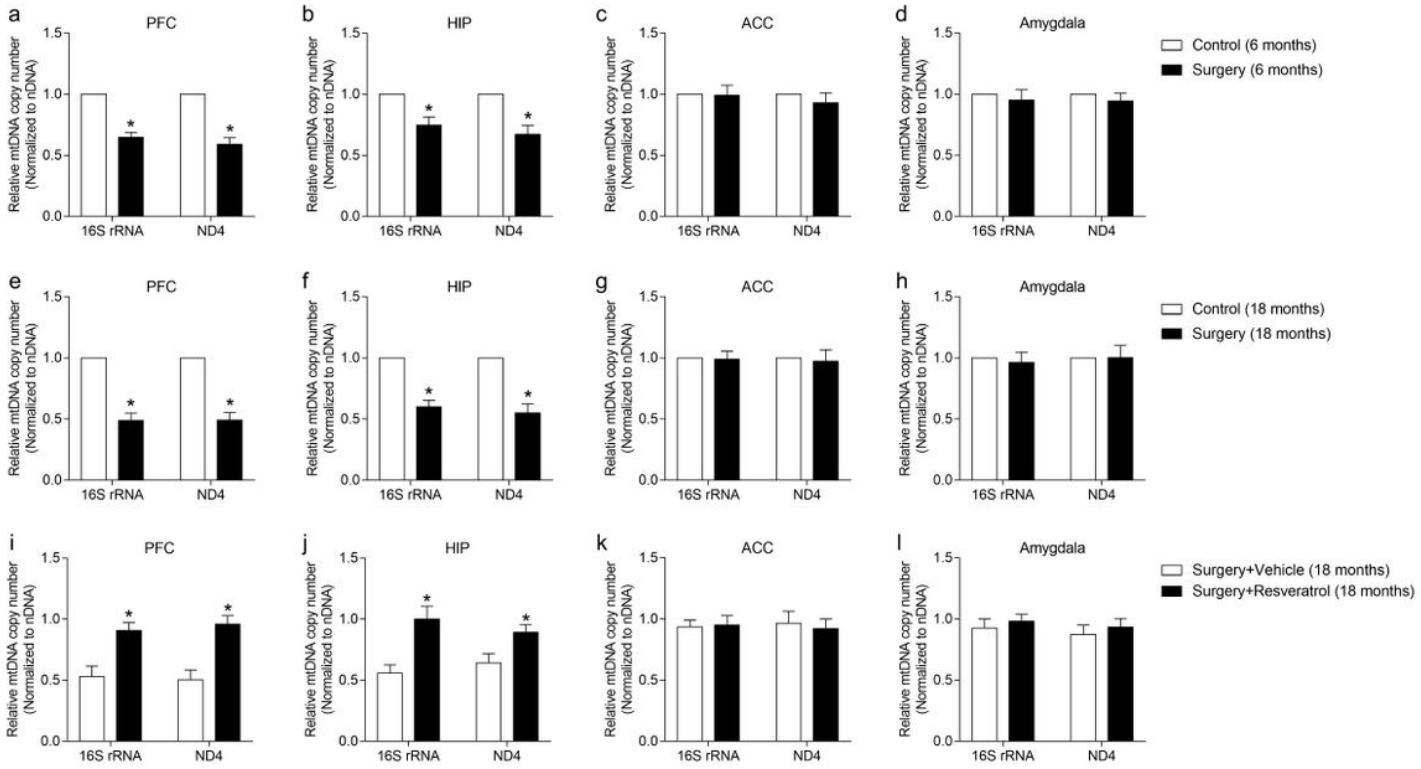


## Figure 4

Relative copy numbers of mtDNA expressed as the ratio of ND4 and 16S rRNA gene copies to 18S rRNA gene copies in the hippocampus, prefrontal cortex, amygdala, and anterior cingulate cortex of (a–d) 6-month-old control mice and mice who underwent surgery, (e–h) 18-month-old control mice and mice who underwent surgery, and (i–l) mice in the 18-month-old surgery + vehicle and surgery + resveratrol groups at 6 h after surgery (n = 5). Data are means ± SDs and were analyzed by one-way ANOVA. *, $P < 0.05$.

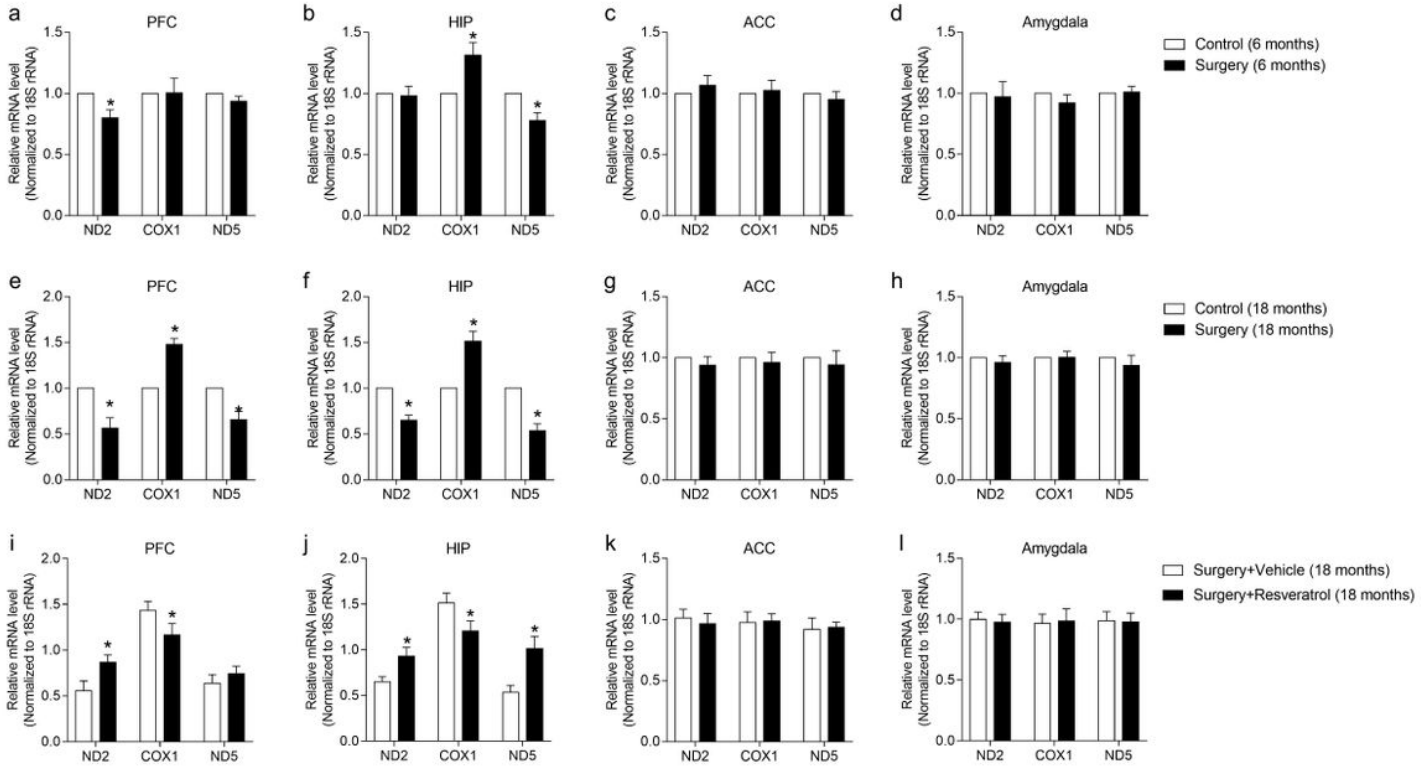


## Figure 5

Relative expression levels of mitochondrial genes (COX1, ND2, ND5) in the hippocampus, prefrontal cortex, amygdala, and anterior cingulate cortex of (a–d) 6-month-old mice in the control and surgery groups, (e–h) 18-month-old mice in the control and surgery groups, and (i–l) 18-month-old mice in the surgery + vehicle and surgery + resveratrol groups at 6 h after surgery (n = 5). Data are means ± SDs and were analyzed by one-way ANOVA. *, $P < 0.05$.

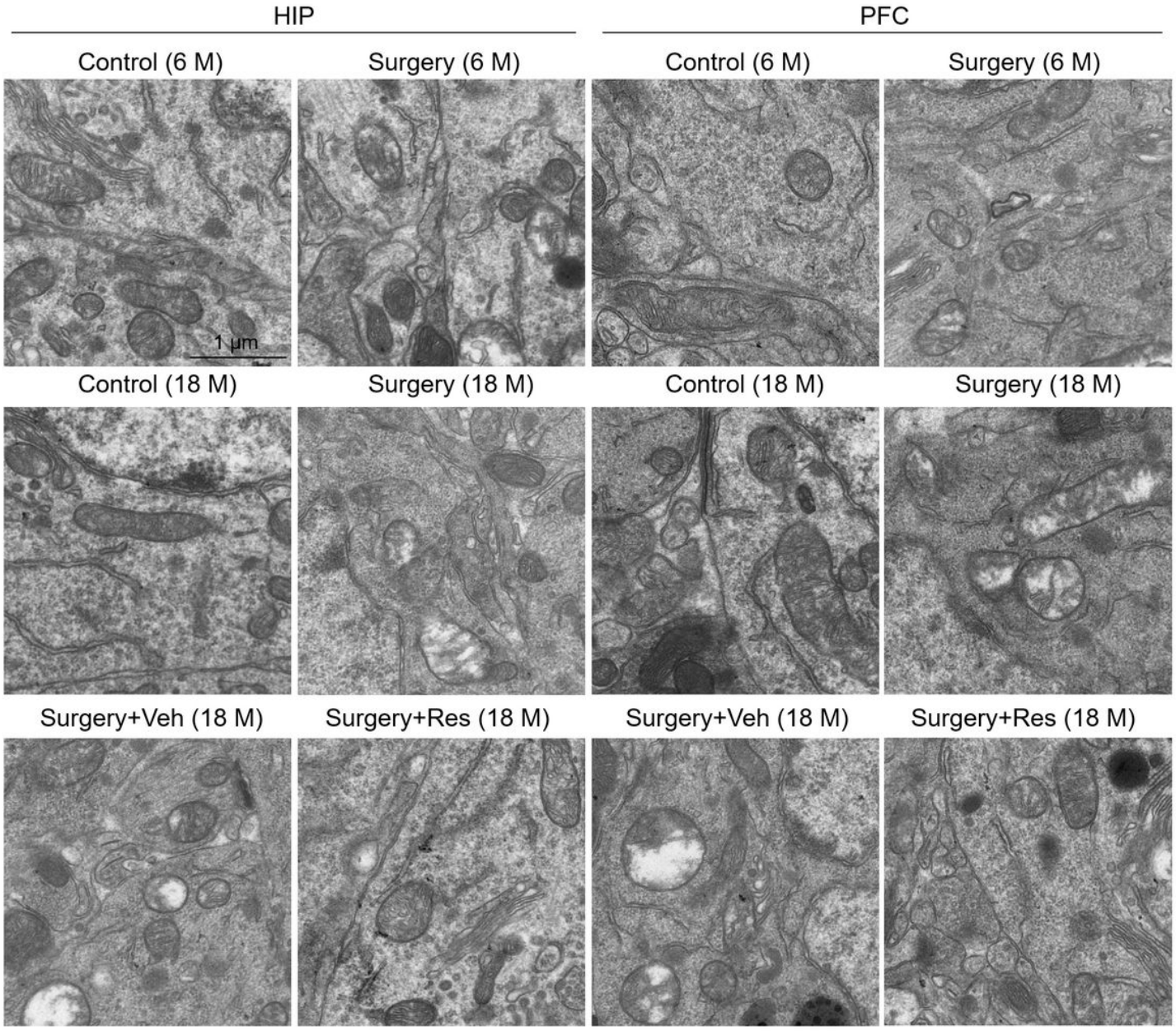


## Figure 6

Ultrastructure changes in mitochondria in neurons form the hippocampus and prefrontal cortex of 6-month-old mice in the control and surgery groups, 18-month-old mice in the control and surgery groups, and 18-month-old mice in the surgery + vehicle and surgery + resveratrol groups at 6 h after surgery. Representative images from the control group showed that mitochondria manifested as long tubules with intact outer and inner membranes and numerous, tightly packed, clear cristae; representative images from the surgery group showed small, round, swollen mitochondria with unclear structures and distorted cristae. Scale bar = 1 μm.

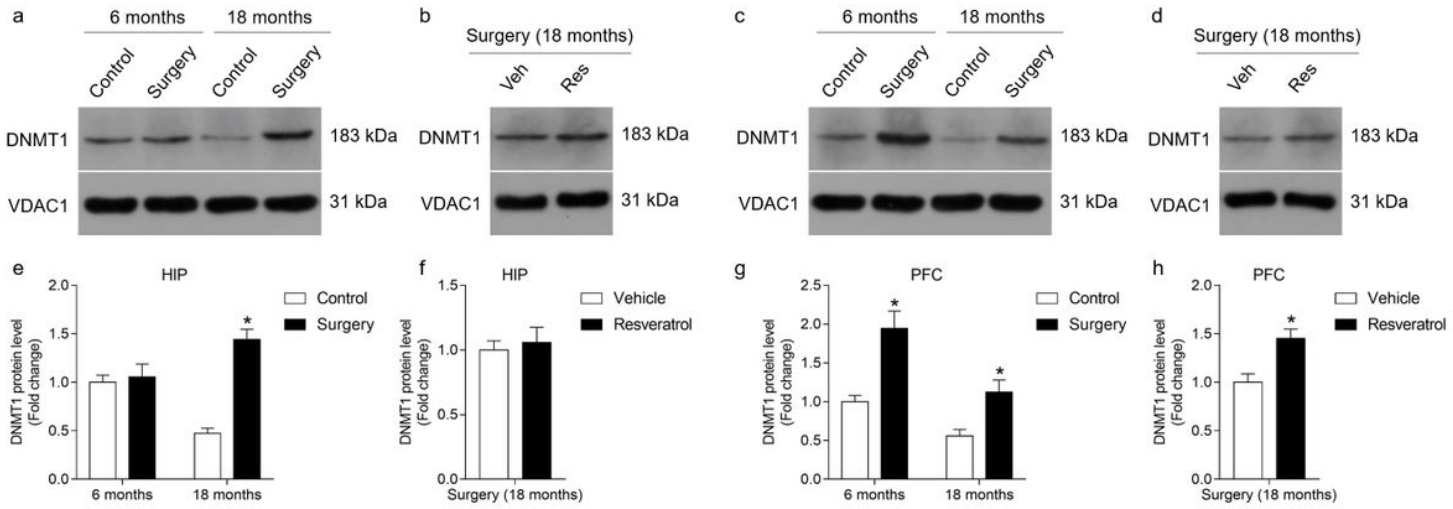


**Figure 7**

Expression levels of mitochondrial DNMT1 in (a, b, e, f) the hippocampus and (c, d, g, h) prefrontal cortex of 6-month-old and 18-month-old mice at 6 h after surgery. (a–d) Western blotting findings for DNMT1 and VDAC1 expression revealed products of 183 and 31 kDa, respectively. (e–h) Densitometric quantification of DNMT1 immunoreactivity on western blots; VDAC1 was used as the loading control (n = 5). Data are means ± SDs and were analyzed by one-way ANOVA. *, P < 0.05.

# Supplementary Files

This is a list of supplementary files associated with this preprint. Click to download.

- supplementalmaterial.docx